



Geant4 simulations of the absorption of photons in CsI and NaI produced by electrons with energies up to 4 MeV and their application to precision measurements of the β -energy spectrum with a calorimetric technique

X. Huyan^{a,b}, O. Naviliat-Cuncic^{a,b,*}, P. Voytas^c, S. Chandavar^a, M. Hughes^{a,b},
K. Minamisono^{a,b}, S.V. Paulauskas^a

^a National Superconducting Cyclotron Laboratory, Michigan State University, East Lansing, MI, USA

^b Department of Physics and Astronomy, Michigan State University, East Lansing, MI, USA

^c Department of Physics, Wittenberg University, Springfield, OH, USA

ARTICLE INFO

Keywords:

Nuclear β decay
Geant4 simulations
CsI
NaI detectors
Bremsstrahlung radiation

ABSTRACT

The yield of photons produced by electrons slowing down in CsI and NaI was studied with four electromagnetic physics constructors included in the Geant4 toolkit. The subsequent absorption of photons in detector geometries used for measurements of the β spectrum shape was also studied with a focus on the determination of the absorption fraction. For electrons with energies in the range 0.5–4 MeV, the relative photon yields determined with the four Geant4 constructors differ at the level of 10^{-2} in amplitude and the relative absorption fractions differ at the level of 10^{-4} in amplitude. The differences among constructors enabled the estimation of the sensitivity to Geant4 simulations for the measurement of the β energy spectrum shape in ${}^6\text{He}$ decay using a calorimetric technique with ions implanted in the active volume of detectors. The size of the effect associated with photons escaping the detectors was quantified in terms of a slope which, on average, is respectively -5.4% /MeV and -4.8% /MeV for the CsI and NaI geometries. The corresponding relative uncertainties as determined from the spread of results obtained with the four Geant4 constructors are 0.0067 and 0.0058.

© 2017 Elsevier B.V. All rights reserved.

1. Introduction

Precision measurements of the Fierz interference term in nuclear and neutron decays offer high sensitivity to searches for exotic scalar and tensor couplings contributing to the weak interaction [1,2]. The most direct way to access the Fierz term is through measurements of the shape of the β -energy spectrum and the current challenge is to reach a sensitivity level below 10^{-3} [2]. Measurements of β -energy spectra have mostly been performed using either magnetic spectrometers [3,4] or particle detectors in configurations in which the suitable β emitter was located outside the active volume of a detector [5]. One of the most severe instrumental effects in the detection of β particles for precision measurements is their backscattering from the detector volumes, resulting in significant distortions of the measured spectra [5].

A common tool to describe the backscattering of electrons in matter is offered by the Geant4 toolkit [6]. The performance of Geant4 for the description of backscattering has recently been studied for semiconductor [7,8] and plastic scintillator detectors [9] used in nuclear decays.

Measurements and quantitative analysis have also been carried out in the energy range of neutron decay [10,11]. The misidentification of the electron energy at those energies has motivated the development of backscatter-suppressed spectrometers [12] to reduce the impact of such undesirable effects. The results in Ref. [8] showed that, for semiconductor detectors, the relative intensities in the description of spectra can be reproduced within $\pm 3\%$ in amplitude over selected energy ranges. However, the same studies indicate possible limitations of Geant4 for precision measurements of the shape of β energy spectra. This is illustrated for instance by the presence of marked slopes in Fig. 17 of Ref. [8]. Systematic studies of the Geant4 simulation of electron backscattering, with focus in the low energy range, down to 0.1 keV, have observed a large variability in the performance of all models for the determination of the backscattering fraction [13].

A new calorimetric technique was recently proposed with the aim to eliminate the effect of electron backscattering for measurements of β -energy spectra [14]. In this technique, the suitable β emitter is implanted

* Corresponding author at: National Superconducting Cyclotron Laboratory, Michigan State University, East Lansing, MI, USA.
E-mail address: naviliat@nsl.msu.edu (O. Naviliat-Cuncic).

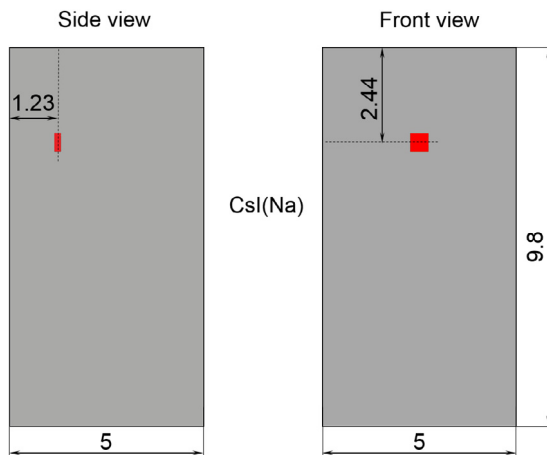


Fig. 1. (Color online) Geometry of the CsI(Na) detector (gray) and position of the electron source (red) used in the simulations. Dimensions are in cm.

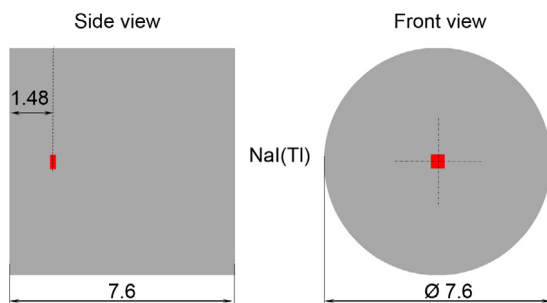


Fig. 2. (Color online) Geometry of the NaI(Tl) detector (gray) and position of the electron source (red) used in the simulations. Dimensions are in cm.

inside a detector and the spectrum is then measured during the decay. Because of the finite detector size, a fraction of the initial β -particle energy escapes the detector through photons, resulting in a distortion of the spectrum shape.

This paper reports on a study of four physics constructors included in Geant4 with the aim to test the variability in the description of photon production and absorption and to estimate the impact of such variability in the analysis of the spectrum shape in ${}^6\text{He}$ decay. The study focuses on the energy absorbed in CsI and NaI materials by electrons produced inside these materials with energies up to 4 MeV.

2. Source and detector geometries

The geometries of the source and detectors used in the simulations are shown in Figs. 1 and 2. They correspond to actual experimental conditions [14] but the description of their achievement is outside the scope of the present study. One detector is a rectangular cuboid $9.8 \times 5 \times 5 \text{ cm}^3$ CsI(Na) scintillator (Fig. 1) and the other is a cylindrical $\text{Ø}7.6 \times 7.6 \text{ cm}^2$ NaI(Tl) scintillator (Fig. 2). The geometry of the electron sources is described by a rectangular cuboid, with dimensions $4.6 \times 4.5 \times 1.5 \text{ mm}^3$ in CsI(Na) and $4.6 \times 4.5 \times 1.7 \text{ mm}^3$ in NaI(Tl). The position of the center of the source in the CsI(Na) detector is 2.44 cm from the top and 1.23 cm deep from the front face. In the NaI(Tl) detector, the source is located on the cylindrical axis at a depth of 1.48 cm from the front face.

3. Geant4 constructors and conditions

Electrons lose energy in CsI and NaI by collision and bremsstrahlung radiation. Collisions include ionization and excitation processes which can give rise to secondary Auger electrons and X-rays. These processes are described in the Geant4 toolkit with various models. The present study used version 10.3.0 of Geant4.

Table 1

Physics lists and constructors of Geant4 used in the present study.

Physics constructors and lists	Denomination
PhysListEmStandard	Standard
G4EmLivermorePhysics	Livermore
G4EmPenelopePhysics	Penelope
G4EmStandardPhysics_option4	Option4

3.1. Geant4 physics constructors

The physics processes are organized in a number of *physics constructors* which implement “electromagnetic physics lists”. Some constructors are adapted to low energy processes and the constructors can sometimes differ by their calculation efficiencies. To test the variability of the results, this study has considered the physics constructors and lists presented in Table 1.

The electromagnetic models included in the physics constructors are described in the Geant4 Physics Reference Manual [15]. In particular, the description of bremsstrahlung are based respectively on the models G4SeltzerBergerModel, G4LivermoreBremsstrahlungModel and G4PenelopeBremsstrahlungModel for the Standard (std), Livermore (liv) and Penelope (pen) constructors. The on-line documentation [16] describes Option4 (opt4) as using the most accurate standard and low-energy models. This constructor is not independent from the other three. The inspection of the source indicates that, for the electron energies considered in this work, it uses G4SeltzerBergerModel for bremsstrahlung. The Standard list is not specifically adapted for low energy processes but has been included here to compare the results with Option4. The actual list used here was taken from Ref. [17]. According to the Physics Reference Manual [15], the constructors optimized for low energies like Livermore and Penelope, use all common data libraries such as the Evaluated Electron Data Library.

3.2. Geant4 geometry

The geometries of the source and detectors described in Section 2 have been implemented in the Geant4 simulations. The selected absorber materials were CsI for the CsI(Na) detector and NaI for NaI(Tl). The primary particle source includes only electrons, uniformly distributed within the volume of the sources inside the detectors (Figs. 1 and 2) and emitted isotropically. Two types of energy distributions for the electrons have been studied: 1) a set of monoenergetic values in the range 0.5–4 MeV and 2) the continuous β spectrum associated with ${}^6\text{He}$ decay which extends up to 3.5 MeV.

An illustration of a simulation with the geometry implementation for the CsI material, with 10^3 events for 1 MeV electrons is shown in Fig. 3. The simulation was performed with the Standard constructor. The electrons (in red) remain inside the detector while some of the photons (in green) escape.

3.3. Geant4 parameters

All default values of parameters used in the physics lists have been adopted. The tracking of primary and secondary particles can be controlled via other parameters. The parameter that controls the creation of secondaries is the range cut (or Cut For Secondaries). The creation occurs if the particle is able to travel over a distance larger than this range in a given material. Otherwise the particle energy is absorbed locally. Unless stated otherwise in the text for specific conditions, the values of the range cuts were fixed to 5.0 μm in CsI and 5.7 μm in NaI for both electrons and photons. For the range factor parameter, F_R , and geometry factor parameter, F_G , [18], which are important for multiple scattering, the default values have been used ($F_R = 0.02$, $F_G = 2.5$ for Penelope, Livermore and Option4 and $F_R = 0.04$ for Standard).

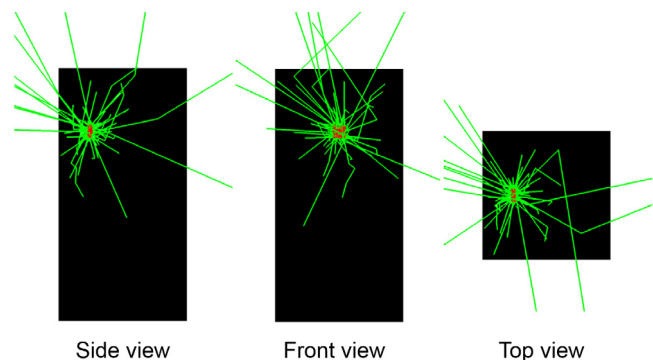


Fig. 3. (Color online) Visualization of a Geant4 simulation with 10^3 events of 1 MeV electrons in the CsI detector. Left: side view of the detector; Middle: front view; Right: top view. The green lines show some of the photons which escape the detector.

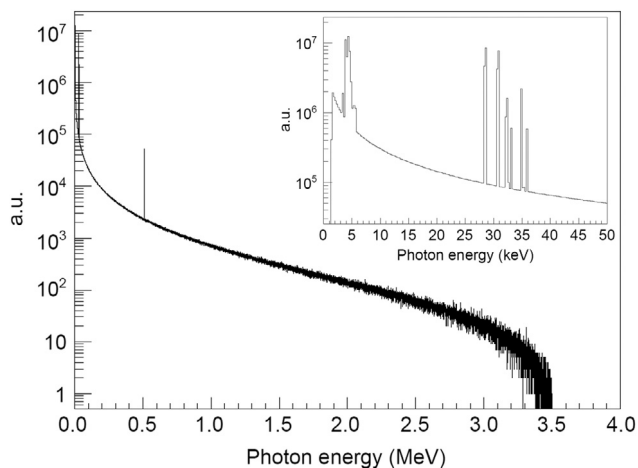


Fig. 4. Photon spectrum produced by 3.5 MeV monoenergetic electrons in CsI detector obtained with the standard constructor.

4. Discrete monoenergetic electrons

The quantification of possible differences in the energy dependence of the production and absorption of photons obtained from the four physics constructors, was performed by studying the response in a material to monoenergetic primary electrons. For illustration, the photon spectrum produced by 3.5 MeV electrons in CsI with the Standard constructor is shown in Fig. 4. The simulation was performed with 2×10^7 generated events. In addition to the bremsstrahlung distribution, the spectrum contains the 511 keV peak from positron annihilation following pair production by high energy bremsstrahlung photons. The insert to Fig. 4 shows the characteristic X-ray lines ($K_{\alpha 1}$, $K_{\alpha 2}$, $K_{\beta 1}$, and K-edge) for I and Cs and also the L-lines at lower energies. When generating similar photon spectra with the other three constructors, it was observed that the atomic processes included in the constructors produce up to 20% relative differences in the intensity of the X-ray peaks, with $I_{\text{pen}} > I_{\text{std}} > I_{\text{liv}} > I_{\text{opt4}}$.

4.1. Photon yield

The production of secondary photons is characterized by the photon yield, Y , which is defined as the fraction of the initial kinetic energy of the primary electrons that is converted into photons. The photon yields for CsI and NaI have been extracted from simulations with primary monoenergetic electrons in the range 0.5–4 MeV in steps of 0.5 MeV. Each simulation used 2×10^7 events.

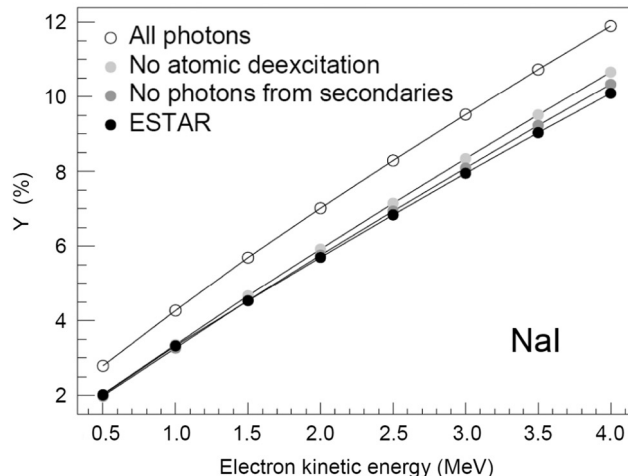
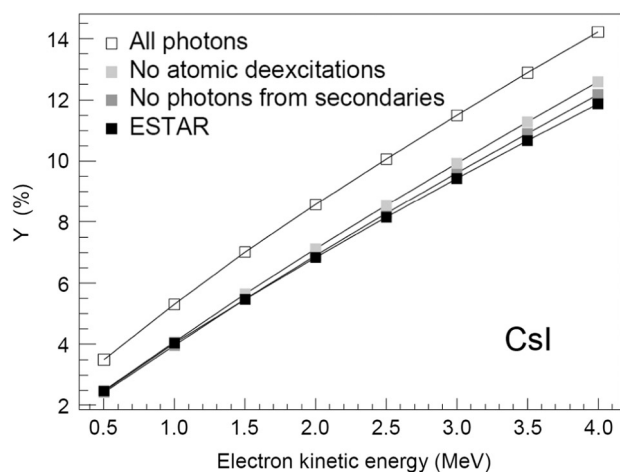


Fig. 5. Photon yields produced in CsI (upper panel) and in NaI (lower panel) as a function of the initial electron energy obtained with the standard constructor. The open, light gray and dark gray markers correspond to Geant4 simulations. The black filled markers are values from the ESTAR tables. See text for details.

The photon yields obtained with the Standard constructor as a function of the initial electron energy are shown in Fig. 5 for CsI and NaI. The open markers (squares and circles) correspond to simulations in which all photon production processes were switched on. In order to understand quantitatively the different sources of secondary photon production, two other settings have been studied. The results with light gray markers were obtained with the atomic deexcitations switched off. These include fluorescence photons, Auger electrons, and Particle Induced X-ray Emission. The dark gray markers are from simulations in which, in addition to disabling atomic deexcitations, the interactions of secondary photons were disabled. These include the photoelectric effect, Compton scattering, and pair production. For this last condition, multiple scattering was also disabled and the range cuts were set to “infinity” (1 km) for electrons and to 3.5 μm and 5 μm for photons in CsI and NaI respectively. The first cut is aimed at reducing secondary photon production by secondary electrons and the second is to fix the photon threshold reasonably low.

From the conditions above, one can deduce the relative contributions of the main photon production mechanisms within the material. It is observed that, after the dominant bremsstrahlung production by the primary electrons, the next largest contribution arises from induced atomic processes followed by bremsstrahlung produced by secondary electrons and positrons. For comparison, the figures also show the values of the radiation yield from the NIST (ESTAR) database (black markers) [19], which is defined as “the average fraction of the initial

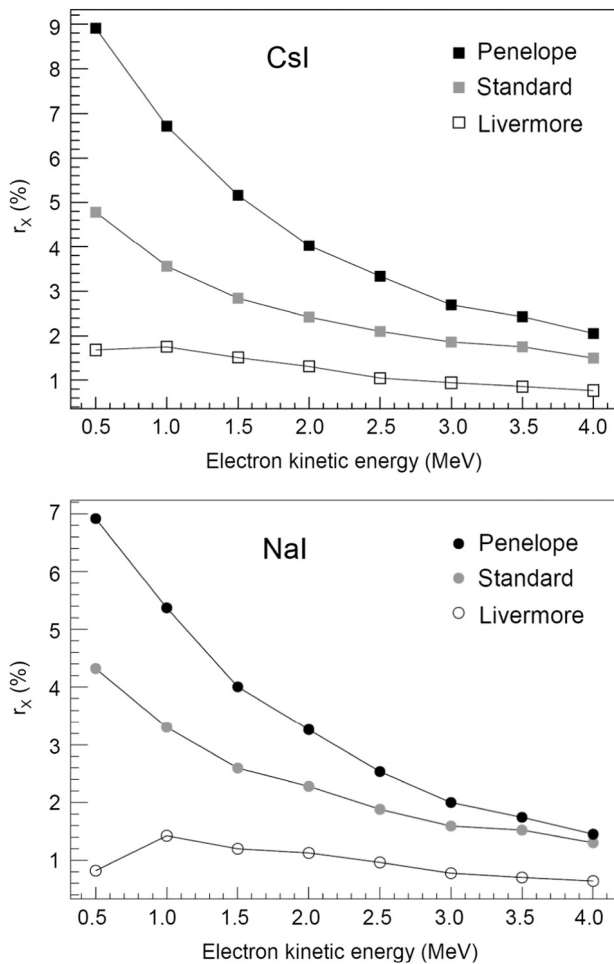


Fig. 6. Relative photon yields produced in CsI (upper panel) and NaI (lower panel) as a function of the initial electron energy obtained with the Penelope (black markers), Standard (gray markers) and Livermore (open markers) constructors. The yields were normalized relative to those calculated with Option4.

kinetic energy of an electron that is converted to bremsstrahlung energy as the particle slows down to rest, calculated in the continuous-slowning-down approximation". The origin of the small but visible difference between the ESTAR tables and the dark gray markers is unclear but can possibly be attributed to details in the calculations of the yields, including the energy integration and cuts, or in differences between the continuous slowing-down approximation and the discrete steps used in Geant4.

In the remainder of this study, all sources of photons are considered since, once produced, any photon has a chance to escape the detector and thereby reduce the deposited energy.

The calculation of the yields with the other three constructors give results that, on the scale of Fig. 5, are undistinguishable from those obtained with the Standard one. To make the differences visible, the yields obtained with three constructors have been normalized to those obtained with Option4. Fig. 6 shows the results of the normalized yields defined as

$$r_X = Y_X/Y_{\text{opt4}} - 1 \quad (1)$$

($X = \text{pen, std, liv}$) for CsI and NaI. For Penelope and Standard, the yields relative to Option4 display a larger energy dependence than for Livermore. The graphs in Fig. 6 also show that for the photon production, the Option4 models appear to be closer to those used by Livermore.

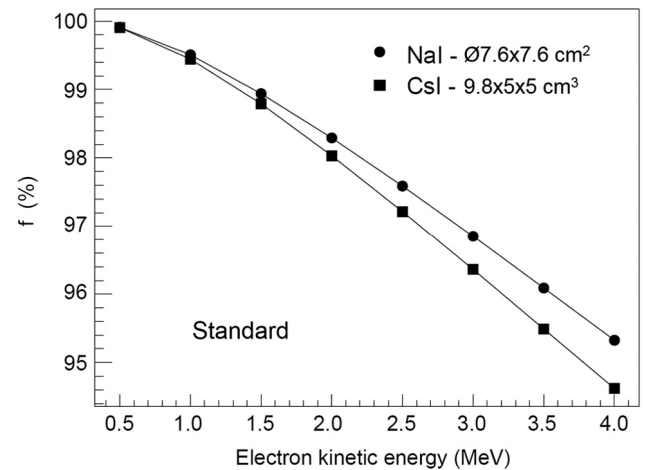


Fig. 7. Absorption fraction as a function of the primary electron energy in NaI (circles) and CsI (squares), calculated with the standard constructor.

Considering an energy of 1.6 MeV as a reference mean value for the analysis of the β -energy spectrum in ${}^6\text{He}$ decay (Fig. 9) it is seen that the yields calculated with the four constructors show a spread of about 5% for CsI and 4% for NaI (Fig. 6). This spread applies to a quantity which has itself a magnitude of about 8% in CsI and 6% in NaI (Fig. 5). If the observed spread is taken as an estimate of the error in the prediction of the photon yield, one can anticipate that the absolute error on the calculated yield would be a few parts in 10^{-3} .

This spread in the photon yield does not imply that a spread of similar magnitude will be present in the total absorbed energy. While the photon yield depends on the electron range in the material, the energy absorbed is strongly related with the geometry of the detector around the electron source. For an infinitely large detector, all photons and hence all energy, will be absorbed.

4.2. Absorption fraction

In analogy with the definition of the photon yield, the absorption fraction, f , is defined here as the fraction of the total kinetic energy of the primary electrons that is absorbed in the detector. Fig. 7 shows the absorption fraction in CsI and NaI as a function of the kinetic energy of electrons calculated with the Standard constructor. Each simulation used 2×10^7 events. It is worth recalling that the geometries of the two detectors are not identical.

Taking again a mean energy of 1.6 MeV from the β spectrum (Fig. 9) it is observed that the average fraction of energy which is not deposited in the detectors is about 1%–2%. This provides an estimate of the average size of the correction, in terms of energy escaping the detector, which is applied to the analysis of the β -particle spectrum. It is seen that the absorption fraction is energy dependent, with a larger fraction escaping the detector as the electron energy increases.

The calculation of the absorption fractions with the other three constructors give results which, on the scale of Fig. 7, are undistinguishable from those obtained with the Standard constructor. To make the differences visible, the fractions obtained with three constructors have again been normalized to those obtained with Option4. Fig. 8 shows the results of the normalized absorption fractions defined as

$$s_X = f_X/f_{\text{opt4}} - 1. \quad (2)$$

The uncertainties on these ratios were deduced from the statistical uncertainties on the mean absorbed energy per event, calculated from the distributions of the absorbed energy spectra.

In contrast to the normalized photon yield (Fig. 6), the normalized absorption fractions do not display a common trend as

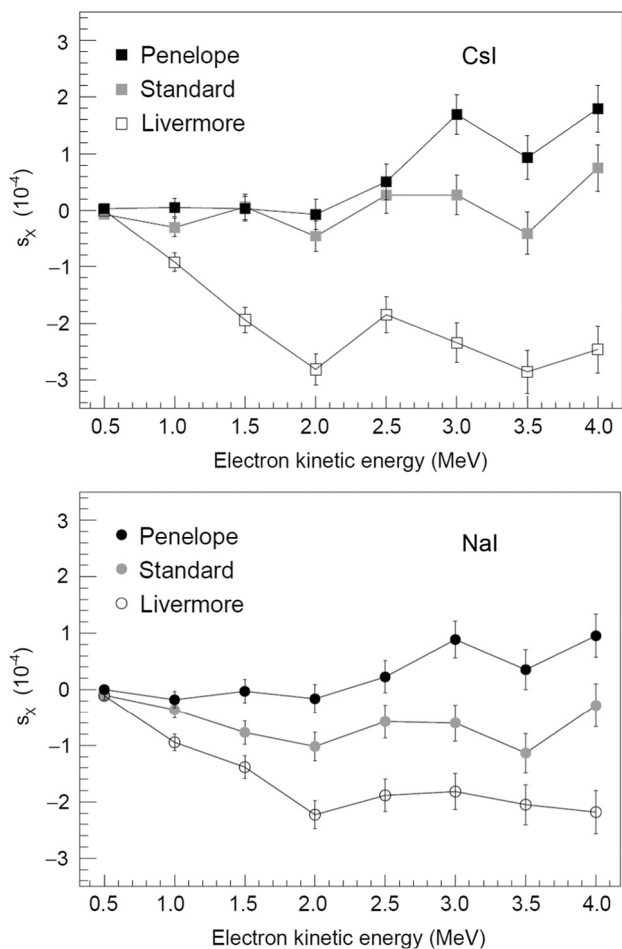


Fig. 8. Relative absorption fraction in CsI (upper panel) and NaI (lower panel) as a function of the initial electron energy obtained with the Penelope (black markers), Standard (gray markers) and Livermore (open markers). The fractions were normalized relative to those obtained with Option4.

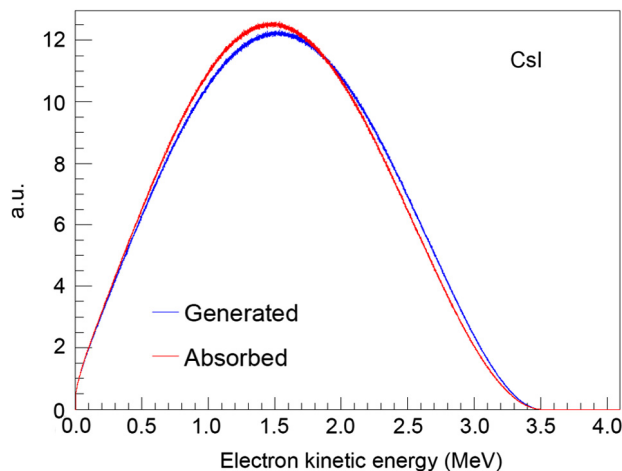


Fig. 9. (Color online) Energy spectra of β particles from ${}^6\text{He}$ decay. Blue: generated spectrum with 10^9 events; Red: spectrum of the energy absorbed in the CsI detector. The simulation was performed with the standard constructor.

a function of the electron energy. Whereas the relative fraction calculated with Penelope increases, the results obtained with Livermore decrease relative to Option4 resulting in a spread that increases with energy. The differences between Option4 and Livermore are larger

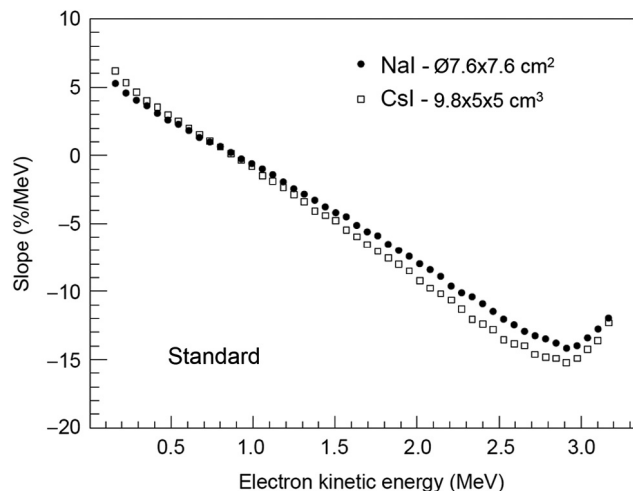


Fig. 10. Numerical derivative of the ratio between the absorbed energy spectrum and the original generated spectrum for the NaI (circles) and CsI (squares) detectors.

than those between Option4 and Penelope, possibly due in part to the fact that Option4 uses the Penelope model for pair production (G4PenelopeGammaConversionModel). The statistical uncertainties are of order 10^{-5} . The spread of a few 10^{-4} in the variation of the relative absorption fractions is two orders of magnitude smaller compared to those of the relative photon yield. Such small differences between the constructors are very difficult to benchmark experimentally. Since the absolute magnitude of the absorption fraction is close to 1, the spread on the calculated relative absorption fractions provides an estimate of the error due to differences in the constructors.

5. Continuous β spectrum

The impact on the analysis of the shape of the β energy spectrum in ${}^6\text{He}$ decay due to possible differences among the Geant4 physics constructors can be directly estimated by generating events following the continuous energy distribution (Fig. 9) instead of using monoenergetic electrons. The spectrum is dominated by the phase space and contains a number of corrections [14] whose details are not relevant within the scope of the present study.

The blue histogram in Fig. 9 was generated following the theoretical β spectrum, with 10^9 events and the red histogram corresponds to the energy absorbed in the CsI detector. For NaI, the differences between the absorbed energy histogram and the undistorted original histogram are smaller.

For the analysis of the shape of the β spectrum, the effect of photons escaping the detector can be estimated by calculating the derivative of the ratio between the absorbed energy spectrum and the original generated spectrum. The values of the derivative are shown in Fig. 10 for the NaI (circles) and CsI (squares) detectors. The slopes vary by a factor of 4 and change sign around 0.9 MeV in kinetic energy. The statistical weight of the region near the end-point energy, where the slopes are largest, is nevertheless smaller than the weight of the central region. The mean values of the slopes deduced from Fig. 10 by weighting them with the squared root of the number of counts in the β spectrum, are -5.4% /MeV for CsI and -4.8% /MeV for NaI. This provides an estimate of the size of the effect on the shape that is being corrected for by the Geant4 simulations.

5.1. Photon yield

The photon yield can be calculated for the continuous β spectrum from the photon spectra simulated with the four constructors. For illustration, Fig. 11 shows the photon spectrum obtained with $2 \times$

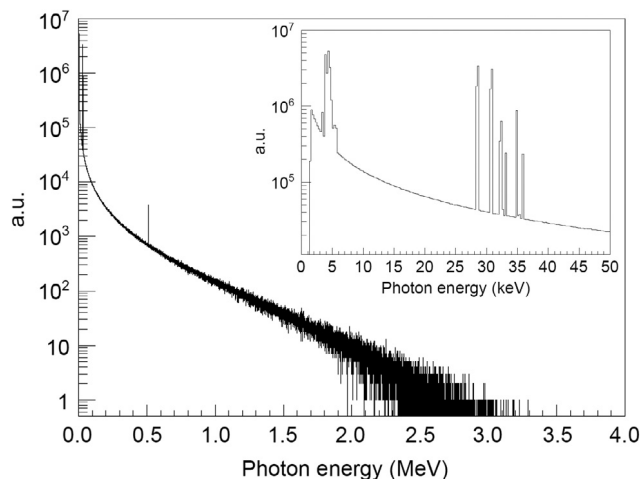


Fig. 11. Photon spectrum produced in CsI by electrons with energies distributed following the β spectrum in ${}^6\text{He}$ decay. The simulation was performed with the standard constructor.

Table 2

Photon yields (in %) produced by electrons with energies following the β spectrum in ${}^6\text{He}$ decay, obtained with four physics constructors.

	Pen	Std	Liv	Opt4
CsI	8.30	8.16	8.07	7.96
NaI	6.75	6.68	6.60	6.53

Table 3

Absorption fraction (in %) produced by electrons with energies following the β spectrum in ${}^6\text{He}$ decay, obtained with four physics constructors.

	Pen	Std	Liv	Opt4
CsI	98.15	98.14	98.12	98.14
NaI	98.39	98.39	98.37	98.39

10^7 generated electrons using the Standard constructor. The salient features are similar to those contained in the spectra generated with monoenergetic electrons (Fig. 4) namely the continuous bremsstrahlung distribution, the 511 keV peak and the X-ray lines.

The photon yields deduced from simulated spectra obtained with the four physics constructors are summarized in Table 2. The values follow the trend observed previously with simulated monoenergetic sources (Figs. 5 and 6), with Penelope giving the largest value, followed by Standard, Livermore and Option4. The largest absolute differences among the calculated yields are 3.4×10^{-3} for CsI and 2.2×10^{-3} for NaI, as anticipated from the results with the monoenergetic sources.

5.2. Absorption fraction

The absorption fractions deduced from simulated spectra obtained with the four physics constructors are given in Table 3. The values follow again the trend observed previously with monoenergetic sources (Figs. 7 and 8). The largest absolute differences among the calculated absorption fractions are 3×10^{-4} for CsI and 2×10^{-4} for NaI, which are both an order of magnitude smaller than the differences among photon yields.

5.3. Comparison of simulated spectra

The spectra of the absorbed energy, similar to the red spectrum in Fig. 9, but obtained with the other constructors are not distinguishable at the scale of that figure. As indicated by the absorption fractions, the differences are expected to be very small so that to quantify them the simulations require high statistics.

For the precise analysis of the shape of the β energy spectrum in the experiment described in Ref. [14], it is possible to estimate the sensitivity to the Geant4 constructors by determining a possible slope in

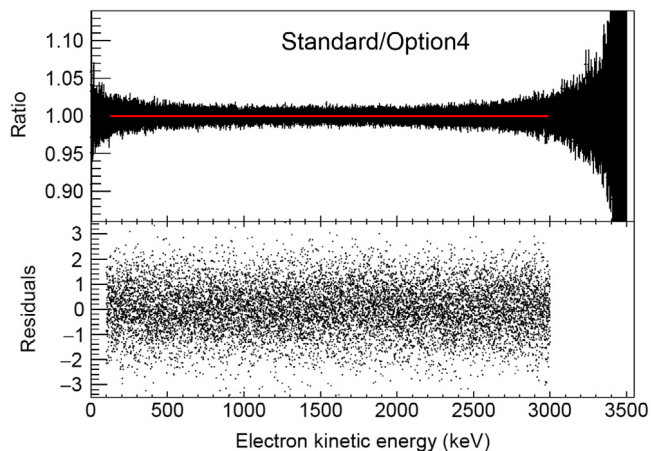


Fig. 12. (Color online) Upper panel: ratio between the absorbed energy spectra simulated with the standard constructor and the Option4 constructor. The red line is a linear fit to the ratio. Lower panel: residuals of the fit.

Table 4

Slopes (in $10^{-8}/\text{keV}$) extracted from the fits of the ratio spectra relative to Option4.

	Pen	Std	Liv
CsI	11.8 ± 6.7	-4.6 ± 6.7	-59.3 ± 6.7
NaI	7.7 ± 6.7	-20.9 ± 6.7	-48.4 ± 6.7

the ratio between simulated spectra. After completing such a procedure, the outcome are then four high statistics spectra for each material. The spectrum obtained with Option4 is taken as reference. The other three spectra (Penelope, Standard and Livermore) are then divided by the spectrum obtained with Option4 and the ratios are fitted with a linear function to search for a possible slope.

The upper panel in Fig. 12 shows the ratio between the Standard and Option4 constructors. The ratio was fitted between 100 and 3000 keV in order to cover an extended energy interval. The lower panel in Fig. 12 shows the residuals of the fit, defined as $(y_{\text{bin}} - y_{\text{fit}})/\sigma_{\text{bin}}$, where y_{bin} and σ_{bin} are respectively the content and error of a bin and y_{fit} is the value of the fitted function at that bin. The slopes extracted from such fits are summarized in Table 4. The uncertainties on the values of the slope correspond to the statistical uncertainty on the linear parameter as returned by the χ^2 minimization and is driven by the statistics in the simulated spectra.

The variation of the slope values are consistent with the observations made with monoenergetic electrons (Fig. 8). From the extreme values of the slopes for each material one can deduce the spreads which are $\pm 3.6(1) \times 10^{-7}/\text{keV}$ for CsI and $\pm 2.8(1) \times 10^{-7}/\text{keV}$ for NaI. This provides an estimate of the sensitivity of the spectrum shape analysis to differences in the constructors. For comparison, these values correspond to respectively 5.5% and 4.3% of the dominant linear term in the shape factor of the β spectrum associated to the weak magnetism form factor [20]. Considering that the size of the effect of photon escape relative to the theoretical spectrum was estimated to be $-5.4 \times 10^{-2}/\text{MeV}$ in CsI and $-4.8 \times 10^{-2}/\text{MeV}$ in NaI, the observed extreme spreads represent a relative uncertainty of respectively 0.67% and 0.58%.

In practice, for the analysis of the shape of the β spectrum in Ref. [14], the simulated spectra are first convoluted with the response function of the detector and then fitted to the data. The impact on the physics results can directly be determined by performing the full analysis with each of the physics constructors. The values estimated above are therefore considered as upper limits of the sensitivity to Geant4 simulations.

6. Conclusions

The variability of four Geant4 physics constructors used to simulate the production and absorption of photons in CsI and NaI has been

investigated. The photons were produced by electrons of up to 4 MeV slowing down in those materials. It was observed that the photon yields calculated with the four physics constructors present relative differences of several percent in amplitude. This is analogous to variabilities observed in the calculations of backscattering fractions [8,13] or in calculations of the differential bremsstrahlung production cross sections [21]. For precision measurements of the shape of the β energy spectrum using a calorimetric technique [14], it is the total absorbed energy which directly affects the response function of detectors. It was observed that the relative spreads of the absorption fractions calculated with the four physics constructors are two orders of magnitude smaller than those from the photon yields. The four constructors differ also in part in the way that atomic processes are treated during the slowing down of electrons. Since the associated emitted photons are low energy, the probability for them to be absorbed in the detectors is relatively large. This makes the measurements using the calorimetric technique significantly less sensitive to details of Geant4 simulations compared to techniques having to deal with backscattering effects.

Acknowledgment

This work is supported by the National Science Foundation (US) under grant number PHY-11-02511.

References

- [1] T. Bhattacharya, V. Cirigliano, S.D. Cohen, A. Filipuzzi, M. González-Alonso, M.L. Graesser, R. Gupta, H.-W. Lin, *Phys. Rev. D* 85 (2012) 054512.
- [2] O. Naviliat-Cuncic, M. González-Alonso, *Ann. Phys. (Berlin)* 525 (2013) 600.
- [3] L.V. Elmbt, J. Deutsch, R. Prieels, *Nucl. Phys. A* 469 (1987) 531.
- [4] E.A. George, P.A. Voytas, G.W. Severin, L.D. Knutson, *Phys. Rev. C* 90 (2014) 065501.
- [5] D. Hetherington, A. Alousi, R. Moore, *Nucl. Phys. A* 494 (1989) 1.
- [6] S. Agostinelli, et al., *Nucl. Instrum. and Methods in Phys. Res. A* 506 (2003) 250.
- [7] F. Wauters, I. Kraev, D. Zákoucký, M. Beck, V. Golovko, V. Kozlov, T. Phalet, M. Tandecki, E. Traykov, S.V. Gorp, N. Severijns, *Nucl. Instrum. and Methods in Phys. Res. A* 609 (2009) 156.
- [8] G. Soti, F. Wauters, M. Breitenfeldt, P. Finlay, I. Kraev, A. Knecht, T. Porobić, D. Zákoucký, N. Severijns, *Nucl. Instrum. and Methods in Phys. Res. A* 728 (2013) 11.
- [9] V. Golovko, V. Iacob, J. Hardy, *Nucl. Instrum. and Methods in Phys. Res. A* 594 (2008) 266.
- [10] J.W. Martin, J. Yuan, S.A. Hoedl, B.W. Filippone, D. Fong, T.M. Ito, E. Lin, B. Tipton, A.R. Young, *Phys. Rev. C* 68 (2003) 055503.
- [11] J.W. Martin, J. Yuan, M.J. Betancourt, B.W. Filippone, S.A. Hoedl, T.M. Ito, B. Plaster, A.R. Young, *Phys. Rev. C* 73 (2006) 015501.
- [12] M. Hassan, F. Bateman, B. Collett, G. Darius, C. DeAngelis, M. Dewey, G. Jones, A. Komives, A. Laptev, M. Mendenhall, J. Nico, G. Noid, E. Stephenson, I. Stern, C. Trull, F. Wietfeldt, *Nucl. Instrum. and Methods in Phys. Res. A* 867 (2017) 51.
- [13] S.H. Kim, M.G. Pia, T. Basaglia, M.C. Han, G. Hoff, C.H. Kim, P. Saracco, *IEEE Trans. Nucl. Sci.* 62 (2015) 451.
- [14] X. Huyan, O. Naviliat-Cuncic, D. Bazin, A. Gade, M. Hughes, S. Liddick, K. Minamisono, S. Noji, S.V. Paulauskas, A. Simon, P. Voytas, D. Weisshaar, *Hyperfine Interact.* 237 (2016) 1.
- [15] Geant4 Physics Reference Manual (2016) <http://geant4.web.cern.ch/geant4/UserDocumentation/UsersGuides/PhysicsReferenceManual/fo/PhysicsReferenceManual.pdf>.
- [16] Physics List EM constructors in Geant4 10.2 (2017) http://geant4.cern.ch/collaboration/working_groups/electromagnetic/physlist10.2.shtml#opt4.
- [17] Source code PhysListEmStandard.cc (2017), Available: http://geant4.web.cern.ch/geant4/UserDocumentation/Doxygen/examples_doc/html_TestEm5/html/PhysListEmStandard_8cc_source.html.
- [18] V.N. Ivanchenko, O. Kadri, M. Maire, L. Urban, *J. Phys. Conf. Ser.* 219 (2010) 032045.
- [19] M. Berger, J. Coursey, M. Zucker, J. Chang, Stopping-Power and Range Tables for Electrons, Protons, and Helium Ions (version 1.2.3), Available: <http://physics.nist.gov/Star>.
- [20] F.P. Calaprice, B.R. Holstein, *Nucl. Phys. A* 273 (1976) 301.
- [21] L. Pandola, C. Andenna, B. Caccia, *Nucl. Instrum. and Methods in Phys. Res. B* 350 (2015) 41.